THE JOURNAL OF PHYSICAL CHEMISTRY B

Article

Cite This: J. Phys. Chem. B XXXX, XXX, XXX−XXX

pubs.acs.org/JPCB

Dynamical Effects in Protein Electrochemistry

Dmitry V. Matyushov*

Department of Physics and School of Molecular Sciences, Arizona State University, PO Box 871504, Tempe, Arizona 85287-1504, United States

Supporting Information

ABSTRACT: Electrochemical measurements of electron transfer from an electrode to proteins immobilized at protective layers of varying thickness have shown the presence of two characteristic regimes: (i) exponential (tunneling) decay of the rate constant with the distance to the electrode and (ii) a plateau region where the rate is independent of the distance to the electrode. The reaction in the plateau region is viewed as friction-controlled electron transfer, with the rate constant inversely proportional to the medium relaxation time. Fitting the rates to established theories requires medium relaxation times far exceeding common estimates and relaxation times obtained from computer simulations of the Stokes-shift dynamics. There is a significant disconnect between experimental observations and theoretical expectations. This difficulty is resolved here by allowing additional dissipative dynamics consisting of protein's low-frequency oscillations in a soft harmonic potential describing binding of the protein to the substrate. Protein translational motions modulate the electrode−protein electronic coupling, leading to a new time-scale appearing, along with the Stokes-shift relaxation time, in the pre-exponential factor of the rate constant. The new model provides a consistent account of the experimental data. The anticipated range of friction-controlled kinetics is significantly extended, since the effective relaxation time entering the rate pre-exponential factor gains an exponential dependence on the mean-square displacement of the protein. Since the mean-square displacement is proportional to temperature, the enthalpy of activation acquires a significant and nontrivial temperature dependence. The possibility of a negative reaction enthalpy is predicted.

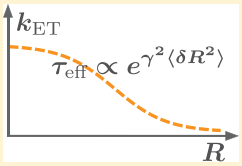

INTRODUCTION

Transport of electrons through chains of redox molecules (cofactors), usually immersed in the protein core, is fundamental for production of biological energy.[1] The protein matrix acts as a catalyst; i.e., it lowers the activation barrier for each elementary electron hop compared to the same reaction in bulk water.[2] The free energy of activation (activation barrier) is the reversible work to reorganize the medium to the tunneling configuration.[3] The free energy of activation is, in turn, affected by two free-energy parameters: the reaction free energy (the difference in free energies between the products and reactants) and the reorganization energy (also a free energy). It is this latter free energy of medium reorganization that is dramatically reduced by the protein compared to solution to allow catalytic action.[4] The reaction free energy is of lesser significance for electron transfer in biology compared to many photoinduced electron-transfer reactions displaying the inverted-region behavior.[5] In contrast, biological electron transfer often occurs in the normal region, with a near-zero reaction free energy.[1] However, altering the free energy of a reaction is important for mechanistic studies of electron transfer,[6] and electrochemistry offers this opportunity through sweeping the electrode potential.[7] This control parameter makes this experimental tool very attractive to access mechanistic properties of protein electron transfer.[8,9] An additional advantage is the ability to directly probe redox properties of the protein active site. This advantage comes in contrast to designs involving an electron donor attached to the surface of the protein.[10] The reorganization energy of electron transfer in these donor−acceptor systems is dominated by the non-native donor exposed to the water solvent.[11]

The probability of electron tunneling between the active site of the protein and the electrode decays exponentially with the distance.[12] This information can be accessed by varying the thickness of the self-assembled monolayer (SAM) placed on the surface of the electrode.[13,14] Such a setup was applied to cytochrome and azurin metalloproteins at gold electrodes covered by alkenethiolates and indeed produced the anticipated exponential decay of the reaction rate with increasing thickness of the SAM.[15−19] However, the exponential falloff was observed only for sufficiently large distances, while the reaction rate plotted as a function of the SAM thickness was found to saturate to a plateau at shorter protein−electrode separations.[15−20] The possibility of gating, i.e., control of the reaction by conformational changes/reorientations at the surface of the monolayer,[20−22] was dismissed by recent measurements involving proteins bound to SAMs.[18,19,23] The current view favors the dynamic, friction-controlled origin of the reaction's crossover from an exponential decay to a plateau region.

The dynamic (friction control) explanation for the observed crossover invokes a general phenomenology of electron-transfer reactions affected by the solvent dynamics.[24−28] Theories of the solvent effect on electron transfer predict that, even for a nonadiabatic reaction with the donor−acceptor

Received: May 13, 2019
Revised: August 1, 2019
Published: August 5, 2019

DOI: 10.1021/acs.jpcb.9b04516
J. Phys. Chem. B XXXX, XXX, XXX−XXX

coupling V below k_BT,[29] the dynamics of barrier crossing becomes affected by Kramers-type diffusion at the top of the activation barrier[30] if the medium is sufficiently slow. To reach this regime, the medium relaxation time has to exceed the time of electron tunneling in the activated state. More precisely, the condition of reaching the regime of dynamical control is determined by the dynamic crossover parameter g. It is given for an electrochemical reaction by the following relation (eq 37 in ref 31)

$$g \simeq 8\tau_x k_B T \Delta/(\hbar\lambda^r) \quad (1)$$

Here, $\Delta = \pi V_\mu^2 \rho_\mu$ is the coupling strength between the reactant and the electrode. It is defined in terms of the electronic coupling V_μ between the electronic state localized on the reactant and the conduction electronic states in the metal. Further, ρ_μ is the density of electronic conduction states at the Fermi level,[32] and V_μ refers to the coupling to the same Fermi-level states. Note that the crossover parameter in eq 37 in ref 31 involves the factor of 4 when diffusional mass transport to the electrode is considered. In contrast, a factor of 8 appears in eq 1 for the crossover parameter in the case of the surface-bound reactant.

In eq 1, λ^r is the effective "reaction" reorganization energy discussed below, which is distinct from the Marcus definition[3] and reflects nonergodic sampling of the configuration space available to the protein on the reaction time.[4] Finally, τ_x is the average Stokes-shift relaxation time[33] representing the decay of the time correlation function of the energy-gap collective reaction coordinate $X(t)$ defined below. The crossover to the solvent dynamical control occurs when $g > 1$, which requires a sufficiently slow decay of dynamical correlations for the nuclear medium modes coupled to the reaction coordinate X (large τ_x in eq 1).

A number of detailed experimental studies performed in recent years have resulted in a consistent phenomenology for the interfacial protein electron transfer.[17−19,34,35] These results can be summarized by the following key observations: (1) There is a crossover in the distance dependence of the reaction rate from an exponential decay at large protein−electrode distances to a plateau at shorter distances. (2) The apparent enthalpy of activation obtained from the Arrhenius plot substantially increases in the plateau region.[18,19,35] The activation enthalpy $\simeq \lambda^r/4$ predicted by the Marcus theory[3] is consistent with the independently measured reorganization energy λ^r at longer distances. (3) The volume of activation changes its sign from negative at long distances to positive at shorter distances, in parallel with an increase in the activation enthalpy.[18] (4) The rate constant correlates with the solvent viscosity η at short distances as $k_{ET} \propto \eta^{-\delta}$, with $\delta \simeq 0.3-0.6$. Some correlation with viscosity is observed for essentially all distances where measurements are possible, up to a tunneling distance of ≃24 Å.[35] The power exponent δ decays with increasing tunneling distance and is essentially zero at the tunneling distances exceeding 24 Å. (5) The activation enthalpy for short distances of electron transfer is strongly affected by the strength of nonspecific hydrophobic attachment of the protein to the SAM.[19] Overall, interactions of proteins with SAMs are weak and nonperturbative, preserving both the structure of the monolayer and the redox potential of the protein.[35] The change of pressure implemented in ref 18 does not substantially affect the viscosity of bulk water. The effect of pressure on electron transfer cannot, therefore, be reduced to changes in bulk viscosity and, instead, points to changes in the protein/SAM relaxation. The mean-square displacement of the bound protein, which becomes a key parameter of the theory proposed here, can depend on pressure and lead to the observable pressure effects.

The consensus reached on the basis of experimental studies is that the crossover occurs in the pre-exponential factor of the rate constant k_{ET} given by the following general equation

$$k_{ET} = k_{NA}/(1 + g) \quad (2)$$

Here, the golden-rule[36] rate constant $k_{NA} \propto \Delta$ decays exponentially with the distance R between the reactant and the electrode

$$\Delta(R) \propto e^{-\gamma R} \quad (3)$$

where the distance decay parameter γ has a typical value[15,19,37] of $\gamma \simeq 1$ Å^{-1}. The subscript "NA", referring to nonadiabatic, points to a narrower usage of this term often found in the literature.[36] In contrast to a more general definition of nonadiabatic transitions, requiring $\Delta > k_BT$,[29] the realm of the golden rule is often viewed as the limit of nonadiabatic transitions.

Since $k_{NA} \propto \Delta$ and $g \propto \Delta$ per eq 1, electronic coupling Δ cancels out in the pre-exponential factor of the rate in eq 2 when $g > 1$. The reaction then crosses over to the friction (dynamics) control of Kramers' reaction kinetics[30]

$$k_{ET} \propto \tau_x^{-1} \quad (4)$$

In this regime, the exponential distance decay of the reaction rate is eliminated and one anticipates a plateau in the rate's dependence on the distance R. For this short-distance plateau, one has to additionally assume $\tau_x \propto \eta^\delta$ to achieve agreement with the reported scaling of the rate with the solvent viscosity.[23,35] However, no connection between the Stokes-shift relaxation time τ_x and solvent viscosity has been established either theoretically or experimentally. Therefore, eq 4 is incapable of explaining the viscosity dependence of the reaction rate. The theory presented below resolves this difficulty.

While the concept of frictional control of the reaction rate agrees qualitatively with the majority of the data, the direct application of eqs 1 and 2 encounters significant difficulties. The reorganization energy of half redox reaction was recently calculated from simulations of cytochrome c (Cyt-c). The value of $\lambda^r \simeq 0.57$ eV from simulations is in perfect agreement with the analysis of cyclic voltammetry data.[38,39] In parallel, the relaxation time for the Stokes-shift dynamics was calculated as $\tau_x \simeq 300-900$ ps in the temperature range 280−360 K. Even though this dynamics is obviously much slower than the longitudinal polarization dynamics with the relaxation time $\tau_L \simeq 0.2$ ps used as τ_x for homogeneous reactions in water,[24,40] it is still too fast to allow the dynamic solvent control according to eq 1. The electronic coupling parameter extracted from fitting the measured rate turns out to be $\Delta \sim 10^{-8}$ eV for the SAM thickness in the crossover region. If this value is combined with τ_x from simulations, $g \simeq 2 \times 10^{-2}$ in eq 2 cannot produce the turnover to the friction-dominated regime. An effective relaxation time of $\tau_x \simeq 188$ ns was estimated to allow the turnover.[12,23] The discrepancy between the typical time-scales of Stokes-shift relaxation in proteins on the one hand and the requirements to fit the experimental data on the other hand points to a major disconnect between the basic phenomenology reported experimentally and the theoretical

DOI: 10.1021/acs.jpcb.9b04516
J. Phys. Chem. B XXXX, XXX, XXX−XXX

framework used to justify the observations (eqs 1 and 2). The equations offered to resolve this contradiction[17,35] are not applicable to the experimental configuration of an immobilized protein, as we discuss in more detail below.

A new theory for the dynamical control of electrochemical reaction rates presented here seeks to resolve the theory/experiment disagreement in terms of an additional dynamic process affecting the reaction rate. Oscillations of the protein attached to the SAM-covered electrode via a soft harmonically restraining potential are considered in addition to the standard polarization dynamics entering established theories of dynamical control of electron transfer.[24−28,40] Diffusional dynamics with the diffusion coefficient D_R modulates the electronic coupling between the reactant and the electrode on the characteristic length γ^{-1} (eq 3). One therefore anticipates that, in addition to the Stokes-shift relaxation time τ_s, the time-scale related to the dynamics of R should affect the reaction rate

$$\tau_\gamma = (\gamma^2 D_R)^{-1} \tag{5}$$

The theory presented below indeed finds that this relaxation time appears, under a specific separation of magnitudes of τ_s and τ_γ, in the pre-exponential factor of the rate constant for the friction-controlled reactions. In that regime, eq 4 changes to

$$k_{ET} \propto \tau_\gamma^{-1} \tag{6}$$

The range of the friction-controlled regime for the reaction is extended when soft binding of the protein to the electrode is introduced. The reason is that the parameter Δ in eq 1 is replaced with

$$\Delta_e \exp[(3\gamma^2/2)\langle \delta R^2 \rangle] \tag{7}$$

where Δ_e refers to the equilibrium electrode−protein separation and $\langle \delta R^2 \rangle$ is the variance of the protein displacement in the soft harmonic attachment (we use a short-hand notation, $\langle \delta R^2 \rangle = \langle (\delta R)^2 \rangle$ and $\langle \delta X^2 \rangle = \langle (\delta X)^2 \rangle$, for the variances along the coordinates R and X, respectively). Increasing $\langle \delta R^2 \rangle$, that is, allowing softer binding of the protein, broadens the range of parameters (such as the distance to the electrode) for which the friction-controlled reaction should be observed. In addition, the mean-square displacement is expected to scale linearly with temperature, $\langle \delta R^2 \rangle \propto T$, according to the fluctuation−dissipation theorem.[41] This explicit temperature dependence adds a temperature-dependent component[42] to the activation free energy $\Delta F^{\dagger}(T)$, which modifies both the entropy and enthalpy of activation.

PHYSICAL MODEL

Models of electron-transfer reactions in solution consider dynamics along two reaction coordinates bringing the system to the top of the activation barrier: the solvent dynamics and the intramolecular dynamics. Along these lines, the Sumi−Marcus model,[25] as well as the two-dimensional diffusion model by Bicout and Szabo,[43] consider the progress of the reacting system along two independent classical coordinates, X for the solvent and Q for intramolecular vibrational motions. Rescaling of these coordinates, $X \to x$ and $Q \to q$, leads to a simple linear condition for the line of the transition state: $x + q$ = Const. The reaction rate is given in terms of the reactive flux across this line.

The situation is somewhat different for electrode reactions. In addition to the polarization coordinate x and intramolecular coordinates, the population dynamics along the distance to the electrode R describes mass transport. For slow diffusion, the current is dominated by the diffusional mass transport, while, for slow electron transfer, it is dominated by the electrode reaction. Even though diffusional dynamics does not bring the system to the transition state, it nevertheless affects the time decay of the electrode current in response to a step of the electrode potential.

The model adopted here describes an electrochemical experiment in which the reactant (redox protein) is immobilized at the surface of the electrode and mass transport does not need to be considered. The reactant is initially in the oxidized (Ox) state, and it accepts the electron from the metal electrode following a step change of the metal overpotential at $t = 0$

$$\mathrm{Ox} + \mathrm{e} \rightarrow \mathrm{Red} \tag{8}$$

Our goal is to determine the time evolution of the surface density $\Gamma(t)$ of the Ox state such that $\Gamma(0) = \Gamma_0$.

The protein is typically bound to the interface either through a surface linker[17] or through a nonspecific hydrophobic attachment.[19] In both cases, one can consider binding as a soft harmonic potential with the force constant κ restraining the protein around the equilibrium distance R_e. For protein electron transfer, the active site is often rigid and does not allow a significant internal reorganization energy (estimated in the range ∼0.05−0.09 eV for Fe-porphins[10,44] and ∼0.1 eV for azurins[45]). In the case of Cyt-c, the analysis of NMR order parameters for Ox and Red states has indicated a significant rigidity of the protein projecting to a low value of the internal reorganization energy.[46] The rigid structure of the active site also drives the Franck−Condon vibrational modes to the quantum domain. This fact makes even small internal reorganization energy irrelevant for the kinetics. Since most protein redox reactions occur in the electron-transfer normal region,[3] intramolecular reorganization of quantum vibrational modes mostly does not affect the activation barrier of protein electron transfer.[4,47] This is illustrated in Figure 1, which shows that the vibrationally excited vibronic surfaces need to be populated to allow activated transitions with lower activation barriers. Since populations $n_v \propto v \exp[-\beta\hbar\omega_v(v + 1/2)]$ of vibronic surfaces with vibrational quantum numbers $v > 0$ tend to zero for quantum vibrations with $\beta\hbar\omega_v \gg 1$ ($\beta = (k_B T)^{-1}$ is the inverse temperature and ω_v is the vibrational

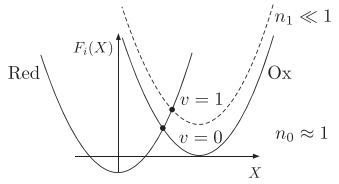

Figure 1. Free energy surfaces $F_i(X)$ (i = Ox, Red) of protein electron transfer along the solvent reaction coordinate X (eq 10). The lower Ox surface indicates the vibrationally ground state $v = 0$, and the upper Ox state indicates the first vibrationally excited state $v = 1$. Since $n_0 \simeq 1$ and $n_1 \ll 1$, the vibrationally excited states are not populated for quantum vibrations $\beta\hbar\omega_v \gg 1$ ($\beta = (k_B T)^{-1}$). Therefore, only the crossing of the lower surfaces with $v = 0$ contributes substantially to the overall rate in the normal region of electron transfer. The rate is determined by the sum over all vibronic channels (indicated by filled circles) weighted with the corresponding vibrational populations.

DOI: 10.1021/acs.jpcb.9b04516
J. Phys. Chem. B XXXX, XXX, XXX−XXX

frequency), there is essentially no contribution of the vibrationally excited states to the reaction rate. The vibrationally excited states of the final (Red) electronic state produce higher activation barriers and also do not contribute. This is what distinguishes the electron-transfer normal region from the inverted region, for which vibrational excitations of the final electronic state (Red in Figure 1) lower the barrier.

The only effect of the quantum modes on the rate in the normal region is to alter the coupling strength Δ' to

$$\Delta = \Delta' e^{-S-S_e} \tag{9}$$

Here, $S = \lambda_v/\hbar\omega_v$ is the Huang–Rhys factor[47,48] determined in terms of the effective vibrational frequency ω_v and the vibrational reorganization energy λ_v. An additional quantum correction[49] $S_e = \mu_e/\hbar\omega_e$ appears from the adiabatic exclusion of the electronic degrees of freedom of the solvent with the characteristic excitation energy ω_e; μ_e is the chemical solvation potential of the reactant by these fast degrees of freedom contributing to the electronic polarization of the medium. These quantum Franck–Condon corrections are assumed to be incorporated in the electronic coupling strength Δ.

On the basis of these considerations, we do not need to consider vibrations of the active site and can simplify the model for barrier passage dynamics by assuming that a single reaction coordinate is sufficient to reach the transition state. This reaction coordinate represents thermal fluctuations of the polarizable medium (protein and water) interacting with the charges of the active site. The difference of these Coulomb interactions in the Red and Ox states leads to the reaction coordinate[24,50]

$$X = \int_\Omega d\mathbf{r}\delta\mathbf{P}\cdot\Delta\mathbf{E}_0 \tag{10}$$

Here, $\delta\mathbf{P}$ is the fluctuation of the polarization density out of equilibrium and the integral is taken over the volume Ω occupied by the polarizable medium (protein excluding the active site[51] and water). Further, $\Delta\mathbf{E}_0$ is the difference of the electric fields of the protein's active site in the final (Red) and initial (Ox) states (including the image effects in the metal electrode).

The variance of X defines the medium reorganization energy[52] λ through the relation

$$\sigma_x^2 = \langle\delta X^2\rangle = 2k_BT\lambda \tag{11}$$

This variance reorganization energy should not be confused with the reaction reorganization energy[53] λ^r as explained below. One can further introduce the dimensionless coordinates[25] $x = X/\sigma_x$ and $z = \delta R/\sigma_R$, where $\delta R = R - R_e$ and

$$\sigma_R^2 = \langle\delta R^2\rangle = (\beta\kappa)^{-1} \tag{12}$$

The resulting two-dimensional harmonic well is described by the harmonic potential of x and z

$$\beta V(x,z) = \frac{1}{2}x^2 + \frac{1}{2}z^2 \tag{13}$$

The free-energy barrier for protein electron transfer is distinct from the rules of the Marcus theory established for homogeneous electron-transfer reactions in polar solvents. The distinction comes from the fact that sampling of the configuration space by proteins is nonequilibrium (nonergodic)[4,54] and thus requires two separate reorganization energies, λ^{St} and λ, for the location of the transition state. This requirement is a special case of a general phenomenology of violation of the fluctuation–dissipation relation[55] in systems out of equilibrium,[56] which also include glassy systems incapable of complete sampling of their phase space.

The relevant parabolic free-energy surfaces along the reaction coordinate X are illustrated in Figure 2 for a reaction

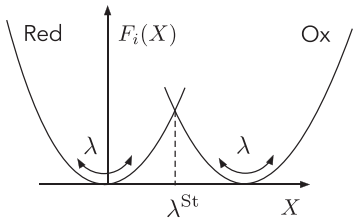

Figure 2. Free energy surfaces $F_i(X)$ (i = Ox, Red) of protein electron transfer along the reaction coordinate X (eq 10) reflecting the modulation of the protein electronic states by fluctuations of the medium (protein and water) polarization. The position of the transition state is characterized by the Stokes-shift reorganization energy λ^{St}, and the curvatures of the parabolas are given by variance reorganization energies λ (eq 11). The activation barrier is $\lambda^r/4$, where the reaction reorganization energy λ^r is given by eq 15. The configuration shown in the plot corresponds to zero electrode overpotential in electrode reactions.

with zero reaction free energy (zero overpotential in electrochemistry[7]). The separation between the parabolas' minima $X_{0,i}$ is $2\lambda^{St} = |X_{0,Ox} - X_{0,Red}|$. Correspondingly, the horizontal distance from the free-energy minimum to the transition state along X is given by the Stokes-shift reorganization energy λ^{St}, which carries an analogy to the Stokes shift between absorption and emission maxima for electronic transitions.[53] A separate reorganization energy λ describes the variance of X or, in other words, the curvature of the parabolas (eq 11). This reorganization energy can be measured from inhomogeneous broadening of optical transition lines.

The change of the perspective from the one dictated by the statistical Gibbs ensemble to the picture of insufficient (nonergodic) sampling does not affect the Marcus energy-gap law, which is based solely on the Gaussian statistics of the energy-gap fluctuations. One therefore obtains for the activation barrier of an electrochemical reaction[4,53]

$$\Delta F^\ddagger = \frac{(\lambda^r + e\varphi)^2}{4\lambda^r} \tag{14}$$

where φ is the electrode overpotential[7] and e is the elementary charge. However, the definition of the reaction reorganization energy λ^r in terms of the energy-gap reaction coordinate X changes from $\lambda = \lambda^{St} = \lambda^r$ in the Gibbs statistics to[4,53]

$$\lambda^r = (\lambda^{St})^2/\lambda \tag{15}$$

specific to nonergodic sampling. Only this parameter, and not λ^{St} and λ separately, can be reported by the electrochemical experiment.[57] It is easy to see from Figure 2 that the activation barrier at $\varphi = 0$ becomes

$$\Delta F^\ddagger = \frac{X^2}{4\lambda}\bigg|_{X=\lambda^{St}} = \frac{(\lambda^{St})^2}{4\lambda} = \frac{\lambda^r}{4} \tag{16}$$

Even though the two reorganization energies λ^{St} and λ are not directly accessible by electrochemistry, the new definition of the observable reorganization energy λ^r is important, since it

DOI: 10.1021/acs.jpcb.9b04516
J. Phys. Chem. B XXXX, XXX, XXX−XXX

explains $\lambda \gg \lambda^r$ typically produced by numerical atomistic simulations and allows one to reconcile simulations with experiment. For instance, the experimental value $\lambda^r \simeq 0.57$ eV for cytochrome c comes from[57] $\lambda^{St} = 1.26$ eV and $\lambda = 2.85$ eV used in eq 15. Equation 15 recovers the standard theory when full sampling is achieved and $\lambda^{St} = \lambda$. In a general case, $\lambda^{St} \leq \lambda$ is required by thermodynamics.[4]

In terms of the scaled reaction coordinate x, the crossing of the free energy surfaces occurs at

$$x_0 = \sqrt{\beta\lambda^r/2} + \phi \tag{17}$$

where $\phi = e\varphi/\sigma_x$ is the scaled value of the electrode overpotential. The transition state x_0 is achieved by diffusional, overdamped dynamics reflecting the many-particle thermal fluctuations of the medium polarization. Each trajectory along the x coordinate is modified by overdamped diffusion along the coordinate z modulating the tunneling probability (Figure 3). Concerted fluctuations of the medium, both bringing the reactant closer to the electrode and shifting its energy level into resonance with one of the filled electronic states of the metal, are those which provide the highest values of the electrode current and thus dominate in the reaction rate.

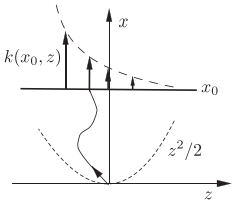

Figure 3. Illustration of the diffusional dynamics in (x, z) space bringing the system to the transition state x_0 (shown schematically by a single trajectory). The rate of tunneling in the transition state is $k(x_0, z)$ (eq 18). It exponentially decays with the scaled distance to the electrode $z = R/\sigma_R$, $\sigma_R^2 = \langle\delta R^2\rangle$ and is modulated by fluctuations of the reactant's position relative to the electrode. A soft harmonic penalty is imposed on fluctuations along the z-coordinate.

With the replacement of the Fermi distribution of the metal electrons with a step function, any $x > x_0$ corresponds to the barrierless tunneling of the electron from the conduction band to the oxidized state of the reactant. The rate of such transitions is described by the Fermi golden rule as

$$k(x, z) = s(z)\theta(x - x_0) \tag{18}$$

where $s(z) = 2\Delta(z)/\hbar$ and $\theta(x)$ is a Heaviside step function.

The functionality for the tunneling rate adopted here assumes that translation, modulating the tunneling distance, is the main nuclear mode responsible for protein mobility at the surface of the SAM. For proteins immobilized through electrostatic binding, protein rotations become an additional source of thermal noise affecting tunneling.[58] The formalism presented below can potentially apply to these scenarios provided the functional form for the dependence of electronic coupling on the angle of rotation is available and these motions can be projected on harmonic fluctuations of the distance R to the electrode. In the absence of this functionality, we turn to the mathematical formulation of the present physical model in terms of a two-dimensional stochastic (Fokker–Planck) equation with the population sink specified by eq 18.

THEORY

The overall dynamics of the reactant density $n(x, z, t)$ is determined by diffusion along the coordinates x and z and the sink of the reactant population given through $k(x, z)$.[25,59] The diffusional dynamics is described by the corresponding Fokker–Planck equation, which for our purposes is more convenient to write in the Hamiltonian form

$$\partial_t \bar{n} = -[H + k]\bar{n} \tag{19}$$

Here, $\bar{n}(x, z)$ is scaled from the original density by the square-root of the equilibrium distribution function

$$\bar{n}(x, z, t) = n(x, z, t)\exp[\beta V(x, z)/2] \tag{20}$$

The Hamiltonian function in eq 19 is easily derived from the Fokker–Planck equation for diffusion in a two-dimensional quadratic potential[60] and is given by the following relation

$$H = H_x + H_z \tag{21}$$

where

$$H_y = -\tau_y^{-1}\left[\frac{\partial^2}{\partial y^2} - \frac{y^2}{4} + \frac{1}{2}\right] \tag{22}$$

and $y = x, z$. The relaxation time τ_x represents Stokes-shift dynamics along the reaction coordinate X (eq 10), and $\tau_z = \tau_R = \langle\delta R^2\rangle/D_R$ is the characteristic diffusion time. We now proceed to solving eq 19 by applying the Sumi–Marcus formalism,[25] which involves an approximate decoupling of certain dynamic correlations in the Green function for the time evolution of $\bar{n}(x, z, t)$.

Dynamic Equation. We adopt the notations by Sumi and Marcus[25] casting the solution of the dynamic evolution equation in terms of bra and ket vectors. Specifically, we will introduce the equilibrium state

$$\langle x, z|e\rangle = [\Gamma_0/(2\pi)]^{1/2}\exp[-\beta V(x, z)/2] \tag{23}$$

where Γ_0 is the equilibrium surface density of the Ox form at the electrode (number of particles per unit area). The normalization of the inner product is obviously

$$\langle e|e\rangle = \Gamma_0 \tag{24}$$

Assuming that the surface density of the reactant is at equilibrium at $t = 0$, the evolution of the system described by the ket vector $|\bar{n}(t)\rangle$ is given by the equation

$$\partial_t|\bar{n}(t)\rangle = -(H + k)|\bar{n}(t)\rangle \tag{25}$$

The ket $|\bar{n}(t)\rangle$ is defined as

$$\langle x, z|\bar{n}(t)\rangle = (2\pi/\Gamma_0)^{1/2}\bar{n}(x, z, t) \tag{26}$$

This definition results in the initial condition $|\bar{n}(0)\rangle = |e\rangle$ if equilibrium is assumed at $t = 0$:

$$n(x, z, 0) = \Gamma_0/(2\pi)\exp[-\beta V(x, z)] \tag{27}$$

One also obtains the time-dependent surface density $\Gamma(t)$ by taking the bra-ket

$$\langle e|\bar{n}(t)\rangle = \Gamma(t) \tag{28}$$

By performing the Laplace transform, one gets the equation for Laplace-transformed state $|\bar{n}(s)\rangle$

$$|\bar{n}(s)\rangle = G(s)|e\rangle \tag{29}$$

where

DOI: 10.1021/acs.jpcb.9b04516
J. Phys. Chem. B XXXX, XXX, XXX−XXX

$$G(s) = [s + H + k]^{-1} \tag{30}$$

is the Green function (resolvent of the operator $H + k$). The Laplace transform of the dynamic surface density $\Gamma(t)$ of the Ox state is the matrix element of the Green function taken with the equilibrium state

$$\Gamma(s) = \langle e|G(s)|e\rangle \tag{31}$$

Correspondingly, the electrode current per unit area is obtained by taking the time derivative of the surface density, $j(t) = -e\,\mathrm{d}\Gamma(t)/\mathrm{d}t$ ($-e$ is the electron charge). The transient current density can be Laplace-transformed to yield

$$j(s) = -e\langle e|sG(s) - 1|e\rangle \tag{32}$$

One can further use the property of the equilibrium states to produce zero eigenvalues, $H|e\rangle = 0$ and $\langle e|H = 0$, to rewrite the above equation as

$$j(s) = e\langle e|kG(s)|e\rangle \tag{33}$$

Equation 33 is formally exact but cannot be calculated for the sink function given by eq 18. In order to come up with a closed-form solution, we employ the decoupling anzatz introduced by Sumi and Marcus.[25] It starts with the exact Dyson equation

$$G(s) = G_0(s) - G_0(s)kG(s) \tag{34}$$

in which $G_0(s) = (s + H)^{-1}$ is the Green function unperturbed by the sink k. It describes diffusional dynamics of the system on the two-dimensional harmonic potential. The decoupling of dynamic correlations in the Sumi−Marcus anzatz consists of projecting out the coupled dynamics of G_0 and G on the equilibrium manifold[25] (also see ref 61)

$$G_0(s)kG(s) \to \langle k\rangle^{-1}G_0(s)k|e\rangle\langle e|kG(s) \tag{35}$$

Here

$$\langle k\rangle = \langle e|k|e\rangle \tag{36}$$

is the average rate of the population decay assuming an equilibrium distribution of the reactant configurations unperturbed by the reaction dynamics (transition-state theory).

From the decoupling approximation, one immediately obtains a closed-form solution for the Laplace-transformed electrode current density[31]

$$j(s) = e\langle k\rangle[s + sa(s)]^{-1} \tag{37}$$

where

$$a(s) = \langle k\rangle^{-1}\langle e|kG_0(s)k|e\rangle \tag{38}$$

The solution for the dynamics of the electrode current is reduced to the calculation of $a(s)$.

Electrode Reaction Rate. The main property required for the calculation of the electrode current and the electrochemical reaction rate is the function $a(s)$ in eqs 37 and 38. It is the Laplace transform of the corresponding time-dependent function

$$A(t) = \langle k\rangle^{-1}\langle e|ke^{-Ht}k|e\rangle \tag{39}$$

The time evolution operator in this equation can be represented by the following bra-ket

$$P(x, z, t; x', z', 0) = \langle x, z|e^{-Ht}|x', z'\rangle \tag{40}$$

which is the well-established propagator of the Ornstein−Uhlenbeck process[60] describing two-dimensional diffusional dynamics in the harmonic potential $V(x, z)$ given by eq 13. The integrals involved in eq 39 are calculated in the Supporting Information. Here we focus on the results of these calculations leading to closed-form solutions for the electrode current and the rate constant of electron transfer.

We start with the equilibrium rate of the electrode reaction $\langle k\rangle$, which is given by the relation

$$\langle k\rangle = \Gamma_0 k_{NA} \tag{41}$$

Here, the golden-rule rate of electrode electron transfer is

$$k_{NA} = \frac{\langle\Delta\rangle}{\hbar}\,\mathrm{erfc}\left[\frac{\lambda^r + e\varphi}{\sqrt{4\lambda^r k_B T}}\right] \tag{42}$$

where $\mathrm{erfc}(x)$ is the complementary error function.[62] The value of the electronic coupling is averaged over the fluctuation of the protein−electrode distance, which enhances the coupling from the equilibrium value Δ_e to the effective coupling[42,63]

$$\langle\Delta\rangle = \Delta_e e^{\gamma^2\langle\delta R^2\rangle/2} \tag{43}$$

Since $\langle\delta R^2\rangle \propto T$ according to the fluctuation−dissipation theorem,[41] soft thermally induced oscillations of the reactant−electrode distance produce temperature-dependent contributions to the enthalpy and entropy of activation.[42]

The time-dependent Ornstein−Uhlenbeck propagator entering eqs 39 and 40 depends on two relaxation times, τ_x and τ_z. This dynamical complexity ensures the complexity of the medium dynamical effect on the rate constant. At large activation barriers, $x_0^2 \gg 1$, one can nevertheless arrive at the exponential decay for the electrode current in response to a step of overpotential at $t = 0$.[64] As is shown in the Supporting Information, the solution is given by the equation[31]

$$j(t) = e\Gamma_0 k_{ET} e^{-k_{ET}t} \tag{44}$$

The rate of population decay k_{ET} is given by eq 2 with k_{NA} from eq 42 and a new definition of the dynamic crossover parameter g

$$g = \tau_{eff}\frac{\langle\Delta\rangle}{\hbar} \tag{45}$$

with

$$\tau_{eff} = 2\tau_\gamma e^{\gamma^2\langle\delta R^2\rangle}h(\tau_x, \tau_\gamma) \tag{46}$$

Here, τ_γ is the characteristic time for translational diffusion over the length of tunneling decay γ^{-1} introduced above (eq 5). This is a new time-scale, which does not appear in the standard formulations of the dynamic effect on electron-transfer kinetics. The appearance of this time-scale is a principal result of this study incorporating protein oscillations modulating the tunneling probability.

The function of two relaxation times $h(\tau_x, \tau_z) < 1$ in eq 46 has the following analytical form

$$h(\tau_x, \tau_\gamma) = 1 - \frac{x_0}{\sqrt{x_0^2 + 4\tau_x/\tau_\gamma}} \tag{47}$$

Depending on relaxation times and the harmonic force constants along the two reaction coordinates, it switches between two dynamical regimes. In the limit $x_0^2 \gg 4\tau_x/\tau_\gamma$, one

DOI: 10.1021/acs.jpcb.9b04516
J. Phys. Chem. B XXXX, XXX, XXX−XXX

can take a series expansion of the square root in the denominator in eq 47. The effective relaxation time becomes

$$\tau_{\mathrm{eff}} = \tau_x \frac{8k_{\mathrm{B}}T}{\lambda^{\mathrm{r}}} e^{\gamma^2\langle \delta R^2\rangle} \tag{48}$$

Combining this equation with eq 45, one arrives at eq 1 in which Δ is replaced with $\langle\Delta\rangle e^{\gamma^2\langle\delta R^2\rangle}$, where $\langle\Delta\rangle$ is given by eq 43

$$g = \frac{8\tau_x k_{\mathrm{B}}T\Delta_{\mathrm{e}}}{\hbar\lambda^{\mathrm{r}}} e^{(3\gamma^2/2)\langle\delta R^2\rangle} \tag{49}$$

Note that accounting for oscillations of the protein relative to the electrode multiplies g in eq 1 with a large factor of $\exp[(3\gamma^2/2)\langle\delta R^2\rangle]$. This alteration of the dynamic crossover parameter significantly widens the range of friction-controlled electrode kinetics. Obviously, the previous result[31] in eq 1 is restored when $\langle\delta R^2\rangle \to 0$.

In the opposite limit ${x_0}^2 \ll 4\tau_x/\tau_\gamma$, one can drop the second term in eq 47 and put $h(\tau_x, \tau_z) \approx 1$. More precisely, for electrode electron transfer from Cyt-*c* discussed in more detail below, molecular dynamics simulations have found[57] $\tau_x(300\ \mathrm{K}) \simeq 750$ ps and $\lambda^{\mathrm{r}} \simeq 0.57$ eV. In addition, the diffusion coefficient of Cyt-*c* in the bulk is[23] $D_R \simeq 8 \times 10^{-7}$ cm^2 s^{-1}. With these estimates and $\gamma \simeq 1.1$ Å^{-1},[15] one obtains the following values: $\tau_\gamma \simeq 100$ ps, $4\tau_x/\tau_\gamma \simeq 28$, and ${x_0}^2 \simeq 11$. Taken together, these estimates applied to eqs 46 and 47 lead to

$$\tau_{\mathrm{eff}} \simeq \tau_\gamma e^{\gamma^2\langle\delta R^2\rangle} \tag{50}$$

As mentioned above, soft harmonic modulation of the distance between the protein's active site and the electrode can be achieved by combined translations and rotations of the protein projected on the *z*-coordinate (Figure 3). Reorientations of the protein electrostatically bound to the SAM were found to occur on a millisecond time-scale.[22] Therefore, τ_γ might be affected by combined rotational−translational dynamics. Keeping in mind that parameters entering eq 45 effectively reflect these dynamic complexities, we discuss below electrochemical kinetic data[17] for Cyt-*c* bound to the SAM by coordination interactions, when protein translations likely dominate. Many potential uncertainties in this analysis have been resolved by our recent molecular dynamics simulations of Cyt-*c* reporting the reorganization energy of the half reaction and the Stokes-shift relaxation time τ_x at a number of temperatures.[57]

Complex Dynamics. The variables $x(t)$ and $z(t)$ described by Ornstein−Uhlenbeck diffusional dynamics are stationary, Gaussian, Markovian stochastic processes characterized by single-exponential time correlation functions with the relaxation times τ_x and τ_z, respectively. The dynamics of the reaction coordinates can be multiexponential or stretched exponential. Accounting for this complication requires an extension to non-Markovian stochastic processes involving memory functions in the corresponding Langevin equations.[65] The Langevin equation propagating the stationary, Gaussian, non-Markovian stochastic process can be transformed into the Fokker−Planck equation for the population dynamics, which gains a time-dependent diffusion coefficient.[65−68] For instance, if one assumes non-Markovian dynamics along the coordinate *z*, eq 22 is generalized to[65]

$$H_z = -\eta_z(t)\left[\frac{\partial^2}{\partial z^2} - \frac{z^2}{4} + \frac{1}{2}\right] \tag{51}$$

where

$$\eta_z(t) = -\frac{\mathrm{d}}{\mathrm{d}t}\ln \chi_z(t) \tag{52}$$

is given in terms of the time autocorrelation function $\chi_z(t) = \langle z(t)z(0)\rangle$. For a Gaussian stochastic variable, the propagator along the coordinate *z* is fully defined[65,67,69,70] in terms of $\chi_z(t)$

$$\langle z|e^{-H_z t}|z'\rangle \propto \exp\left[-\frac{(z - z'\chi_z(t))^2}{2(1 - \chi_z(t)^2)}\right] \tag{53}$$

No higher-order time correlation functions are needed to characterize the dynamics.

The long-time Stokes-shift dynamics is typically exponential, as was found in simulations of Cyt-*c*.[57] Therefore, only the dynamics along the *z*-coordinate potentially requires involvement of memory effects in order to account for experimental power-law scaling of the reaction rate with the solvent viscosity.[23,35] As we show in the Supporting Information, the time-domain function $A(t) = A(0)F(t)$ in eq 39 can be given by the product of

$$A(0) = \frac{2\langle\Delta\rangle}{\hbar} e^{\gamma^2\langle\delta R^2\rangle} \tag{54}$$

and $F(t) = F_x(t)F_z(t)$ such that $F(0) = 1$. The function $F_x(t)$ is given by eq S20 in the Supporting Information and does not require modification from the single-exponential, Markovian case. For the function $F_z(t)$, the application of the non-Markovian propagator in eq 53 results in

$$F_z(t) = \exp[\gamma^2\langle\delta R^2\rangle(\chi_z(t) - 1)] \tag{55}$$

The problem of calculating the electrode current is, therefore, reduced to computing the Laplace transform of $A(t)$ and inverting the Laplace transform of the current in eq 37 to obtain the response to the potential step of the electrode (eq 44).

This procedure leads to a closed-form expression presented in the previous section for the exponential form of $\chi_z(t)$ but cannot be accomplished for an arbitrary time correlation function. A separate closed-form solution is, however, possible for the stretched dynamics

$$\chi_z(t) = \exp[-(t/\tau_z)^\delta] \tag{56}$$

with the stretching exponent $\delta = 1/2$. This type of stretched dynamics in fact provides a fair account of the conformational dynamics projected on the distance between sites in the protein.[71−73] The main question addressed here is whether the non-Markovian dynamics of the reaction coordinate is projected onto the power-law dependence of the rate on the solvent viscosity. We find that there is no fundamental reason to anticipate this connection. Two limits, $\tau_{\mathrm{eff}} \propto \tau_x$ and $\tau_{\mathrm{eff}} \propto \tau_\gamma$, found for the Markovian dynamics, apply to the non-Markovian dynamics with $\delta = 1/2$ as well. However, there is a range of parameters for which the power-law dependence on the solvent viscosity can be a reasonable empirical representation of the data.

We show in the Supporting Information that, when $F_z(t)$ with the correlation function from eq 56 and $\delta = 1/2$ is used to calculate the current $j(t)$ (eq 44), one obtains the rate given by

DOI: 10.1021/acs.jpcb.9b04516
J. Phys. Chem. B XXXX, XXX, XXX−XXX

eqs 2 and 45 with the effective relaxation time modified from eq 48 to the following relation

$$\tau_{\text{eff}} = \tau_x \frac{8k_B T}{\lambda^r} e^{\gamma^2\langle \delta R^2\rangle} f(a) \tag{57}$$

with

$$f(a) = \frac{2}{a^2}\left[\frac{2a}{\sqrt{\pi}} - 2 + (2 - a^2)e^{a^2/4}\,\text{erfc}(a/2)\right] \tag{58}$$

and

$$a = \frac{2\gamma\sqrt{\langle \delta R^2\rangle}}{x_0}\sqrt{\frac{\tau_x}{\tau_\gamma}} \tag{59}$$

When the dynamics along the z-coordinate can be neglected, one has $a \to 0$ and $f(a) \to 1$, thus recovering eq 48. On the other hand, when $a \gg 1$, one gets the asymptote $f(a) \simeq 4/a^2$ and $\tau_{\text{eff}} \propto \tau_\gamma$ recovering eq 50. However, in the range of intermediate values of a, $f(a)$ is well approximated by the equation (Figure S1 in the Supporting Information)

$$f(a) \simeq (1 + a^{3/2})^{-1} \tag{60}$$

and one obtains at $a > 1$

$$\tau_{\text{eff}} \propto e^{\gamma^2\langle \delta R^2\rangle} \tau_x^{1/4} \tau_\gamma^{3/4} \tag{61}$$

In this range of parameters, a measurement altering τ_γ, such as by changing the solvent viscosity, will report a power-law dependence on the parameters affecting the relaxation time. However, this calculation strongly suggests that there is no fundamental significance in the power-law dependence of the rate constant on viscosity. Such a mathematical analysis of the data provides a fair representation, in a limited range of parameters,[74] of a more complex functionality, such as that given by the function $f(a)$ in eq 58. In other words, the fact that $f(a)$ decays with viscosity η slower than $\propto \eta^{-1}$ does not grant fundamental importance to the power law $\propto \eta^{-\delta}$.

RESULTS

The dependence on the protein−electrode electronic coupling Δ disappears from the rate pre-exponential factor in the limit of friction control ($g > 1$) when one gets

$$k_{\text{ET}} = \tau_{\text{eff}}^{-1}\,\text{erfc}\left[\frac{\lambda^r + e\varphi}{\sqrt{4\lambda^r k_B T}}\right] \tag{62}$$

This equation can be directly applied to experimental kinetic data for the reduction of Cyt-c attached to the mixed pyridine-terminated alkenthiol PyC_n/C_{n-1} coating the silver electrode.[17] These kinetic results belong to the plateau region in the dependence of the rate on the SAM thickness. The charge-transfer distance for these SAMs is given in terms of the number n of methylene groups by the following relation:[23] $R \simeq 1.9 + 1.12n$ Å.

The experimental electron-transfer rates measured[17] by time-resolved surface-enhanced Raman spectroelectrochemistry[22] (TR-SERR) are presented by the points in Figure 4. The fact that the rate shows a dependence on the electrode overpotential φ, as expected from standard models of electron transfer,[3] is strong evidence[22] against the gating mechanism in which a conformational transition of the protein is the rate-limiting step.[21] Indeed, a good fit of the experimental data to

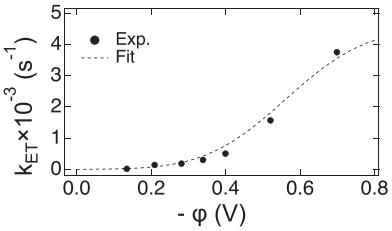

Figure 4. Experimental (Exp.) data for the reduction of Cyt-c[17] on PyC_6/C_5 SAM coating silver electrode (points), T = 298 K. Shown is the dependence of the electron-transfer rate constant on the electrode overpotential φ. The dashed line is the fit to eq 62 with $\tau_{\text{eff}} \simeq 0.45$ ms considered as the fitting parameter. The reaction reorganization energy (eq 15), $\lambda^r(T) = 0.698 - 4.59 \times 10^{-4}T$ (K), is from molecular dynamics simulations,[57] and $\gamma = 1.12$ Å^{-1} is adopted to describe the distance falloff of the electronic coupling (eq 3).

eq 62 is possible with τ_{eff} as the single fitting parameter and λ^r taken from molecular dynamics simulations.[57] While the quality of the fit is encouraging, the resulting relaxation time $\tau_{\text{eff}} \simeq 4.5 \times 10^{-4}$ s is much higher than $\tau_{\text{eff}} \simeq 188$ ns estimated previously[23] and ≃370 ns obtained from our analysis of electrochemical data below. The reasons for the discrepancy between the TR-SERR data and electrochemical kinetics are not entirely clear.[17,58]

Figure 5 shows electrochemical rate constants at T = 298 K reported for PyC_n/C_{n-1} (n = 6, 11, 12, 16) coating gold

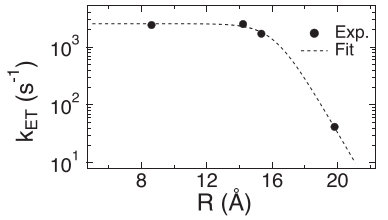

Figure 5. Experimental (Exp.) data for reduction of Cyt-c[17] on PyC_n/C_{n-1} SAM (n = 6, 11, 12, 16) coating the gold electrode (points), T = 298 K. The dashed line is the fit to eq 63 with $\tau_{\text{eff}} \simeq 0.37$ μs. The rest of the parameters are as in Figure 4.

electrodes (points).[17] The dashed line is the fit to the following equation combining eqs 2, 42, and 45

$$k_{\text{ET}} = \frac{\langle\Delta\rangle/\hbar}{1 + \tau_{\text{eff}}\langle\Delta\rangle/\hbar}\,\text{erfc}\left[\frac{\lambda^r + e\eta}{\sqrt{4\lambda^r k_B T}}\right] \tag{63}$$

Fitting the experimental points requires $\tau_{\text{eff}} \simeq 0.37$ μs and $\langle\Delta(n = 11)\rangle = 8.5 \times 10^{-9}$ eV. The fit is done with the fixed γ = 1.12 Å^{-1} while varying τ_{eff} and Δ_0 in $\langle\Delta(R)\rangle = \Delta_0 \exp[-\gamma R]$ as two fitting parameters. As above, the reorganization energy is fixed at the value $\lambda^r \simeq 0.57$ eV from molecular dynamics simulations.[57] If $\tau_\gamma = 10^{-10}$ s estimated above is used in eq 45, the fitted value of τ_{eff} requires the root-mean-square displacement (rmsd) of the protein relative to the SAM equal to $R_{\text{rmsd}} \simeq 2.6$ Å.

Observations consistently show[18,19,23,35] an increase of the apparent activation enthalpy for the standard rate constant $k_0 = k_{\text{ET}}(\varphi = 0)$ in the friction-controlled domain compared to the standard prediction of the Marcus theory, $\Delta H^\dagger \simeq \lambda^r/4$. The increase was attributed to the contribution of the activation energy of the medium relaxation time to the Arrhenius slope.

DOI: 10.1021/acs.jpcb.9b04516
J. Phys. Chem. B XXXX, XXX, XXX−XXX

By applying eq 50, one obtains for the standard rate constant at $\beta\lambda^r \gg 1$ in the friction-controlled region

$$k_0 \approx \frac{1}{\tau_\gamma}\frac{4}{\sqrt{\pi\beta\lambda^r}} e^{-\gamma^2\langle\delta R^2\rangle - \beta\lambda^r/4} \quad (64)$$

If an Arrhenius temperature law is assumed for the relaxation time $\tau_\gamma = \tau_0 \exp[\beta E_s]$, one obtains the apparent activation enthalpy

$$\Delta H^\dagger = \lambda^r/4 + E_s - k_B T\gamma^2\langle\delta R^2\rangle \quad (65)$$

where the temperature dependences of E_s and λ^r are neglected and $\langle\delta R^2\rangle = (\beta\kappa)^{-1}$ (eq 12) was used. Note that λ^r was found to be weakly dependent on temperature in molecular dynamics simulations of Cyt-*c*.[57]

Along the same lines, one obtains an enhancement of the apparent activation enthalpy in the regime of the exponential decay of the rate

$$\Delta H^\dagger_{NA} = \lambda^r/4 + k_B T\gamma^2\langle\delta R^2\rangle/2 \quad (66)$$

The activation enthalpy must always be positive in this regime of the reaction. The second term in this equation is obviously the activation entropy[42]

$$\Delta S^\dagger_{NA}/k_B = \gamma^2\langle\delta R^2\rangle/2 \quad (67)$$

The appearance of E_s in eq 65 accounts for an increase of the activation enthalpy in the friction-controlled regime observed experimentally.[18,19,23,35] The last term in eq 65 is reducing this effect, and it is not negligible: according to the fit of the experimental data in Figure 5, it contributes $\simeq 9k_BT$ to $\Delta H^\dagger$. Since this term grows with increasing temperature, eq 65 anticipates a possibility of a curved Arrhenius plot. A negative apparent activation enthalpy, producing an anti-Arrhenius slope,[75] can potentially be reached at sufficiently high temperatures.

DISCUSSION

The present model combines stochastic Kramers' dynamics[30] along the reaction coordinate X describing the medium polarization[24,50] with the diffusive translational dynamics of the protein in a soft harmonic potential binding it to the electrode. Fluctuations of the protein position modulate the protein−electrode electronic coupling and lead to the appearance of a new characteristic time-scale τ_γ (eq 5) not present in the traditional models of the solvent dynamic effect on electron transfer.[24−28]

Two major outcomes follow from applying the Sumi−Marcus anzatz[25] to calculate the electrode current in response to a step in the electrode potential. First, the relaxation time along the R-coordinate enters the rate pre-exponential factor: τ_γ replaces τ_x appearing in the traditional theories of the dynamic solvent effect.[24−28] Second, the effective relaxation time in eqs 45 and 48 is multiplied by $\exp[\gamma^2\langle\delta R^2\rangle]$, thus making τ_{eff} significantly higher than the relaxation times of the nuclear fluctuations affecting the barrier passage. This factor comes on the top of a purely statistical result $\langle\Delta\rangle = \Delta_e \exp[(\gamma^2/2)\langle\delta R^2\rangle]$ effectively enhancing the electronic coupling from its equilibrium value Δ_e through protein's translational motions. The overall result is a significant enhancement of the crossover parameter g in eq 49 compared to eq 1, where the distance to the electrode was fixed. A low effective relaxation time required to fit the data was the main source of disagreement between the traditional theory and observations, which is resolved in the present formalism. The range of frictional control of the reaction rate is substantially extended compared to traditional models of the solvent dynamical effect on electron transfer.

The analysis of the experimental turnover of the reaction rate with the distance from the electrode (Figure 5) shows that the long relaxation time τ_{eff} required to fit eq 63 can be well accommodated if loose binding to the electrode, with rmsd ∼2−3 Å, is allowed. Separate studies are required to establish if this estimate describes the experimental conditions. Comparison with molecular dynamics simulations[57] shows that τ_{eff} is much longer than the effective time-scale of Stokes-shift dynamics $\tau_x \simeq 300-900$ ps.

Competition between τ_x and τ_γ time-scales in the rate pre-exponential factor (function $h(\tau_x, \tau_\gamma)$ in eq 46) is a result of their close magnitudes: $\tau_\gamma \sim 100$ ps in our estimates. This situation is very different from the relaxation time-scales ∼0.01−0.1 s reported in ref 76. These relaxation times represent the dynamics of single-molecule fluorescence lifetimes of photoexcited flavin adenine dinucleotide quenched through electron transfer from a nearby tyrosine electron donor in flavin reductase. The mathematical model applied to describe this problem assumed modulation of the exponentially decaying tunneling probability by slow donor−acceptor vibrations.[76−78] Their formulation overlaps with the present agenda considering fluctuations of the protein−electrode distance (the electrode is the donor, and Cyt-*c* is the acceptor).

If the model of harmonic donor−acceptor fluctuations with the memory friction, similar to the one considered here, is adopted,[77] the long time-scales reported in ref 76 require an unreasonably high friction of the protein:[72] the friction coefficient from ref 78 is $\zeta \simeq 20$ g/s, while more recent direct measurements of the same property have produced[79] $\zeta \simeq 4 \times 10^{-2}$ g/s. This effective friction is likely to represent population dynamics of the enzyme switching, by overcoming barriers, between active and inactive states[78,80−83] and not necessarily the single-well non-Markovian diffusional dynamics of the variable $R(t)$. In our calculations focused on the response current, a much slower relaxation time disappears from the rate and $k_{ET} \propto \tau_x^{-1}$ when $\tau_\gamma \gg \tau_x$. An additional substantial distinction between the present model and intraprotein distance dynamics studied in ref 76 should be mentioned: the rmsd of the donor−acceptor distance was[78] ∼0.5 Å in their case, while a much softer binding of the protein to the SAM, with the rmsd equal to ∼2.6 Å, is obtained here from fitting the kinetic data in Figure 5. This large rmsd can be a combined effect of the heterogeneous morphology of the SAM, altering the protein−electrode distance, and of the actual protein−SAM binding (electron tunneling rmsd of ≃1 Å was measured for an osmium complex covalently tethered to alkanethiol SAMs of different length[84]). The heterogeneous component of rmsd does not show up in single-molecule measurements, in contrast to the electrochemical setup.

To complete the discussion, we comment on alternative equations used for the analysis of experiment.[17,35] The rate constant k_{ET} derived here describes the decay of the surface population $\Gamma(t)$ and is therefore expressed in the units of inverse time. Zusman[85] suggested to transform this fixed-distance rate constant to the rate constant k_{el} commonly reported for electrode reactions involving mass transport, which has the units of length per time.[7] The transformation is achieved by integrating $k_{ET}(R)$ with the assumed uniform bulk distribution of the reactant: $\rho(R) = \rho_0\theta(R - R_0)$, where ρ_0 is

DOI: 10.1021/acs.jpcb.9b04516
J. Phys. Chem. B XXXX, XXX, XXX−XXX

the bulk concentration. The electrochemical rate constant is then defined as

$$k_{el}\rho_0 = \int_{R_0}^{\infty} dR\rho(R)k_{ET}(R) \quad (68)$$

The result of integration in eq 68 with $k_{ET}(R)$ from eq 63 is

$$k_{el} = (\gamma g_0)^{-1}k_{NA}(R_0)\ln[1 + g_0] \quad (69)$$

where $g_0 = g(R_0)$ in eq 1 and $k_{NA}(R_0)$ is the golden-rule reaction rate in eq 42. This result, assuming a uniform distribution of reactants in solution, does not apply to experiments with reactants attached to the electrode and thus distributed with the one-particle density $\rho(R) \propto \langle\delta(R - R_e)\rangle$, where the average is over the statistical distribution of R. It turns out that eq 69 does not apply either when diffusive mass transport of the reactants to the electrode is allowed. When mass transport is combined[31] with the Kramers diffusional dynamics in the Sumi–Marcus algorithm, simple volume integration does not appear in the solution. The dynamics of mass transport, and not the reaction dynamics, dominates in the electrode current except for the distances closest to the electrode. The solution given by eq 69 does not, therefore, appear in any problem of practical significance.

CONCLUDING REMARKS

Significant disagreement between experimental data for protein electrochemistry and theoretical formalisms developed for reactions in solution became apparent when computer simulations allowed for better constraining of the theory parameters and reducing the flexibility of fitting the data. A theoretical formalism and the analysis of experimental data presented here resolve the theory–experiment disconnect by introducing a new dissipative mode affecting the rate: overdamped oscillations of the protein in a soft harmonic potential binding it to the electrode.

Translational dynamics of the protein modulating the electron tunneling probability has been added to the well-established Kramers-type diffusional dynamics of the medium polarization. Protein's mobility affects the reaction rate by significantly extending the range of friction-controlled electrode kinetics. The new model predicts a nontrivial temperature dependence of the activation enthalpy (eq 65): it can become negative at sufficiently high temperatures, producing an anti-Arrhenius slope when the reaction rate is plotted in the Arrhenius plot vs the inverted temperature.

The principle of weak (transient) binding, allowing protein's release after the reaction, is also realized in biological energy chains, where small redox-active proteins shuttle electrons to larger membrane-bound protein complexes. The physical mechanisms considered here are, therefore, not limited to conditions of electrode reactions. The present theory is maintained for charge transfer between the donor and acceptor connected by a flexible linker or by a binding interaction energy. It predicts that charge transfer will be friction-controlled in a range of donor–acceptor distances and solvent relaxation times significantly extended for flexible complexes compared to the rigid ones.

Similar arguments may apply to intraprotein electron transfer between the donor and acceptor cofactors within a large protein complex (such as reaction centers of photosynthesis) and, potentially, to hopping charge conductivity in proteins.[86] In all of these cases, fluctuations of the distance between the donor and acceptor sites (hopping sites for conductivity), induced by protein viscoelastic motions, will extend the range of friction-controlled electron transfer. This mechanism will prevent, within a certain range of distances, the exponential distance falloff of the charge hopping rate in complete analogy with the picture shown in Figure 5.

ASSOCIATED CONTENT

Supporting Information

The Supporting Information is available free of charge on the ACS Publications website at DOI: 10.1021/acs.jpcb.9b04516.

Derivation of the electrode current in terms of polarization and vibration reaction coordinates (eq 46) and derivation of eq 58 for complex dynamics (PDF)

AUTHOR INFORMATION

Corresponding Author

*E-mail: dmitrym@asu.edu. Phone: (480)965-0057.

ORCID

Dmitry V. Matyushov: 0000-0002-9352-764X

Notes

The author declares no competing financial interest.

ACKNOWLEDGMENTS

This research was supported by the National Science Foundation (CHE-1800243). The author is grateful to David Waldeck for useful comments on the manuscript.

REFERENCES

(1) Nicholls, D. G.; Ferguson, S. J. *Bioenergetics 3*; Academic Press: London, 2002.

(2) Warshel, A.; Sharma, P. K.; Kato, M.; Xiang, Y.; Liu, H.; Olsson, M. H. M. Electrostatic basis for enzyme catalysis. *Chem. Rev.* **2006**, *106*, 3210–3235.

(3) Marcus, R. A.; Sutin, N. Electron transfer in chemistry and biology. *Biochim. Biophys. Acta, Rev. Bioenerg.* **1985**, *811*, 265–322.

(4) Matyushov, D. V. Fluctuation relations, effective temperature, and ageing of enzymes: The case of protein electron transfer. *J. Mol. Liq.* **2018**, *266*, 361–372.

(5) Barbara, P. F.; Meyer, T. J.; Ratner, M. A. Contemporary issues in electron transfer research. *J. Phys. Chem.* **1996**, *100*, 13148–13168.

(6) Closs, G. L.; Miller, J. R. Intramolecular long-distance electron transfer in organic molecules. *Science* **1988**, *240*, 440–447.

(7) Bard, A. J.; Faulkner, L. R. *Electrochemical Methods. Fundamentals and Applications*, 2nd ed.; Wiley: New York, 2001.

(8) Léger, C.; Bertrand, P. Direct electrochemistry of redox enzymes as a tool for mechanistic studies. *Chem. Rev.* **2008**, *108*, 2379.

(9) Alvarez-Paggi, D.; Hannibal, L.; Castro, M. A.; Oviedo-Rouco, S.; Demicheli, V.; Tórtora, V.; Tomasina, F.; Radi, R.; Murgida, D. H. Multifunctional cytochrome *c*: Learning new tricks from an old dog. *Chem. Rev.* **2017**, *117*, 13382–13460.

(10) Winkler, J. R.; Gray, H. B. Electron flow through metalloproteins. *Chem. Rev.* **2014**, *114*, 3369–3380.

(11) Blumberger, J. Free energies for biological electron transfer from QM/MM calculation: method, application and critical assessment. *Phys. Chem. Chem. Phys.* **2008**, *10*, 5651–5667.

(12) Gray, H. B.; Winkler, J. R. Long-range electron transfer. *Proc. Natl. Acad. Sci. U. S. A.* **2005**, *102*, 3534–3539.

(13) Chidsey, C. E. D. Free energy and temperature dependence of electron transfer at the metal-electrolyte interface. *Science* **1991**, *251*, 919–922.

(14) Finklea, H. O. Electrochemistry of organized monolayers of thiols and related molecules on electrodes. *Electroanalytical Chemistry: A Series of Advances* **1996**, *19*, 109–335.

DOI: 10.1021/acs.jpcb.9b04516
J. Phys. Chem. B XXXX, XXX, XXX–XXX

(15) Chi, Q.; Zhang, J.; Andersen, J. E. T.; Ulstrup, J. Ordered assembly and controlled electron transfer of the blue copper protein azurin at gold (111) single-crystal substrates. *J. Phys. Chem. B* **2001**, *105*, 4669−4679.
(16) Fujita, K.; Nakamura, N.; Ohno, H.; Leigh, B. S.; Niki, K.; Gray, H. B.; Richards, J. H. Mimicking protein−protein electron transfer: Voltammetry of pseudomonas aeruginosa azurin and the thermus thermophilus CuA domain at ω-derivatized self-assembled-monolayer gold electrodes. *J. Am. Chem. Soc.* **2004**, *126*, 13954−13961.
(17) Yue, H.; Khoshtariya, D.; Waldeck, D. H.; Grochol, J.; Hildebrandt, P.; Murgida, D. H. On the electron transfer mechanism between cytochrome *c* and metal electrodes. Evidence for dynamic control at short distances. *J. Phys. Chem. B* **2006**, *110*, 19906−19913.
(18) Khoshtariya, D. E.; Dolidze, T. D.; Shushanyan, M.; Davis, K. L.; Waldeck, D. H.; van Eldik, R. Fundamental signatures of short- and long-range electron transfer for the blue copper protein azurin at Au/SAM junctions. *Proc. Natl. Acad. Sci. U. S. A.* **2010**, *107*, 2757.
(19) Monari, S.; Battistuzzi, G.; Bortolotti, C. A.; Yanagisawa, S.; Sato, K.; Li, C.; Salard, I.; Kostrz, D.; Borsari, M.; Ranieri, A.; et al. Understanding the mechanism of short-range electron transfer using an immobilized cupredoxin. *J. Am. Chem. Soc.* **2012**, *134*, 11848−11851.
(20) Avila, A.; Gregory, B. W.; Niki, K.; Cotton, T. M. An electrochemical approach to investigate gated electron transfer using a physiological model system: Cytochrome *c* immobilized on carboxylic acid-terminated alkanethiol self-assembled monolayers on gold electrodes. *J. Phys. Chem. B* **2000**, *104*, 2759−2766.
(21) Jeuken, L. J. C. Conformational reorganisation in interfacial protein electron transfer. *Biochim. Biophys. Acta, Bioenerg.* **2003**, *1604*, 67−76.
(22) Murgida, D. H.; Hildebrandt, P. Disentangling interfacial redox processes of proteins by SERR spectroscopy. *Chem. Soc. Rev.* **2008**, *37*, 937−945.
(23) Waldeck, D. H.; Khoshtariya, D. E. *Applications of Electrochemistry and Nanotechnology in Biology and Medicine I*; Springer: New York, 2011; pp 105−238.
(24) Zusman, L. D. Outer-sphere electron transfer in polar solvents. *Chem. Phys.* **1980**, *49*, 295−304.
(25) Sumi, H.; Marcus, R. A. Dynamical effects in electron transfer reactions. *J. Chem. Phys.* **1986**, *84*, 4894−4914.
(26) Rips, I.; Jortner, J. Dynamic solvent effects on outer-sphere electron transfer. *J. Chem. Phys.* **1987**, *87*, 2090−2104.
(27) Hynes, J. T. Outer-sphere electron-transfer reactions and frequency-dependent friction. *J. Phys. Chem.* **1986**, *90*, 3701−3706.
(28) Yan, Y. J.; Sparpaglione, M.; Mukamel, S. Solvation dynamics in electron-transfer, isomerization, and nonlinear optical processes: a unified Liouville-space theory. *J. Phys. Chem.* **1988**, *92*, 4842−4853.
(29) Frauenfelder, H.; Wolynes, P. G. Rate theories and puzzles of hemeprotein kinetics. *Science* **1985**, *229*, 337−345.
(30) Kramers, H. Brownian motion in a field of force and the diffusion model of chemical reactions. *Physica* **1940**, *7*, 284−304.
(31) Matyushov, D. V. Potential-step transient response of an electrochemical system. *J. Electroanal. Chem.* **1994**, *367*, 1−6.
(32) Schmickler, W.; Santos, E. *Interfacial Electrochemistry*, 2nd ed.; Springer: Berlin, 2010.
(33) Maroncelli, M. The dynamics of solvation in polar liquids. *J. Mol. Liq.* **1993**, *57*, 1−37.
(34) Khoshtariya, D. E.; Dolidze, T. D.; Zusman, L. D.; Waldeck, D. H. Observation of the turnover between the solvent friction (overdamped) and tunneling (nonadiabatic) charge-transfer mechanisms for a Au/Fe$(CN)_6^{3-/4-}$ electrode process and evidence for a freezing out of the Marcus barrier. *J. Phys. Chem. A* **2001**, *105*, 1818−1829.
(35) Zitare, U. A.; Szuster, J.; Scocozza, M. F.; Espinoza-Cara, A.; Leguto, A. J.; Morgada, M. N.; Vila, A. J.; Murgida, D. H. The role of molecular crowding in long-range metalloprotein electron transfer: Dissection into site- and scaffold-specific contributions. *Electrochim. Acta* **2019**, *294*, 117−125.
(36) Levich, V. G. In *Advances in Electrochemistry and Electrochemical Engineering*; Delahay, P., Ed.; Interscience: New York, 1965; Vol. *4*, pp 1−124.
(37) Newton, M. D.; Smalley, J. F. Interfacial bridge-mediated electron transfer: mechanistic analysis based on electrochemical kinetics and theoretical modelling. *Phys. Chem. Chem. Phys.* **2007**, *9*, 555−572.
(38) Cheng, J.; Terrettaz, S.; Blankman, J. I.; Miller, C. J.; Dangi, B.; Guiles, R. D. Electrochemical comparison of heme proteins by insulated electrode voltammetry. *Isr. J. Chem.* **1997**, *37*, 259−266.
(39) Wei, J. J.; Liu, H.; Niki, K.; Margoliash, E.; Waldeck, D. H. Probing electron tunneling pathways: Electrochemical study of rat heart cytochrome *c* and its mutant on pyridine-terminated SAMs. *J. Phys. Chem. B* **2004**, *108*, 16912−16917.
(40) Gayathri, N.; Bagchi, B. Quantum and non-markovian effects in the electron transfer reaction dynamics in the Marcus inverted region. *J. Phys. Chem.* **1996**, *100*, 3056−3062.
(41) Hansen, J.-P.; McDonald, I. R. *Theory of Simple Liquids*, 4th ed.; Academic Press: Amsterdam, The Netherlands, 2013.
(42) Matyushov, D. V. Electron transfer in molecules with conformational transitions. *Chem. Phys. Lett.* **1993**, *203*, 131−136.
(43) Bicout, D. J.; Szabo, A. Electron transfer reaction dynamics in non-Debye solvents. *J. Chem. Phys.* **1998**, *109*, 2325−2338.
(44) Sigfridsson, E.; Olsson, M. H. M.; Ryde, U. A comparison of the inner-sphere reaorganization energies of cytochromes, iron-sulfur clusters, and blue copper proteins. *J. Phys. Chem. B* **2001**, *105*, 5546−5552.
(45) Cascella, M.; Magistrato, A.; Tavernelli, I.; Carloni, P.; Rothlisberger, U. Role of protein frame and solvent for the redox properties of azurin from *Pseudomonas aeruginosa*. *Proc. Natl. Acad. Sci. U. S. A.* **2006**, *103*, 19641−19646.
(46) Liu, W.; Rumbley, J. N.; Englander, S. W.; Wand, A. J. Fast structural dynamics in reduced and oxidized cytochrome c. *Protein Sci.* **2009**, *18*, 670−674.
(47) Bixon, M.; Jortner, J. Electron transfer − From isolated molecules to biomolecules. *Adv. Chem. Phys.* **2007**, *106*, 35−202.
(48) Huang, K.; Rhys, A. Theory of light absorption and non-radiative transitions in F-centres. *Proc. R. Soc. London Ser. A* **1950**, *204*, 406−423.
(49) Matyushov, D. V.; Ladanyi, B. M. Dispersion solute-solvent coupling in electron transfer reactions. I. Effective potential. *J. Chem. Phys.* **1998**, *108*, 6362−6377.
(50) Warshel, A. Dynamics of reactions in polar solvents. Semiclassical trajectory studies of electron-transfer and proton-transfer reactions. *J. Phys. Chem.* **1982**, *86*, 2218−2224.
(51) Dinpajooh, M.; Martin, D. R.; Matyushov, D. V. Polarizability of the active site of cytochrome *c* reduces the activation barrier for electron transfer. *Sci. Rep.* **2016**, *6*, 28152.
(52) Marcus, R. A. On the theory of electron-transfer reactions. VI. Unified treatment for homogeneous and electrode reactions. *J. Chem. Phys.* **1965**, *43*, 679−701.
(53) Matyushov, D. V. Protein electron transfer: Dynamics and statistics. *J. Chem. Phys.* **2013**, *139*, 025102.
(54) Matyushov, D. V. Protein electron transfer: is biology (thermo)dynamic? *J. Phys.: Condens. Matter* **2015**, *27*, 473001.
(55) Kubo, R. The fluctuation-dissipation theorem. *Rep. Prog. Phys.* **1966**, *29*, 255−284.
(56) Kurchan, J. In and out of equilibrium. *Nature* **2005**, *433*, 222−225.
(57) Seyedi, S.; Waskasi, M. M.; Matyushov, D. V. Theory and electrochemistry of cytochrome *c*. *J. Phys. Chem. B* **2017**, *121*, 4958−4967.
(58) Ly, H. K.; Martí, M. A.; Martin, D. F.; Alvarez-Paggi, D.; Meister, W.; Kranich, A.; Weidinger, I. M.; Hildebrandt, P.; Murgida, D. H. Thermal fluctuations determine the electron-transfer rates of cytochrome *c* in electrostatic and covalent complexes. *ChemPhysChem* **2010**, *11*, 1225−1235.

DOI: 10.1021/acs.jpcb.9b04516
J. Phys. Chem. B XXXX, XXX, XXX−XXX

(59) Tang, J.; Marcus, R. A. Diffusion-controlled electron transfer processes and power-law statistics of fluorescence intermittency of nanoparticles. *Phys. Rev. Lett.* **2005**, *95*, 107401−4.
(60) Gardiner, C. W. *Handbook of Stochastic Methods*; Springer: Berlin, 1997.
(61) Bian, Y.; Wang, Z.; Chen, A.; Zhao, N. Fluctuating bottleneck model studies on kinetics of DNA escape from α-hemolysin nanopores. *J. Chem. Phys.* **2015**, *143*, 184908−8.
(62) Abramowitz, M., Stegun, I. A., Eds. *Handbook of Mathematical Functions*; Dover: New York, 1972.
(63) Borgis, D. C.; Lee, S.; Hynes, J. T. A dynamical theory of nonadiabatic proton and hydrogen atom transfer reaction rates in solution. *Chem. Phys. Lett.* **1989**, *162*, 19−26.
(64) Henstridge, M. C.; Laborda, E.; Rees, N. V.; Compton, R. G. Marcus−Hush−Chidsey theory of electron transfer applied to voltammetry: A review. *Electrochim. Acta* **2012**, *84*, 12−20.
(65) Fox, R. F. The generalized Langevin equation with Gaussian fluctuations. *J. Math. Phys.* **1977**, *18*, 2331−2335.
(66) Hänggi, P. Correlation functions and masterequations of generalized (non-Markovian) Langevin equations. *Z. Phys. B: Condens. Matter Quanta* **1978**, *31*, 407−416.
(67) Dong, W.; Andre, J. C. Diffusion-controlled reactions. II. An approach based on a generalized diffusion equation. *J. Chem. Phys.* **1994**, *101*, 299−306.
(68) Chaudhury, S.; Cherayil, B. J. Complex chemical kinetics in single enzyme molecules: Kramers's model with fractional Gaussian noise. *J. Chem. Phys.* **2006**, *125*, 024904−10.
(69) Wang, M. C.; Uhlenbeck, G. E. On the theory of the Brownian motion II. *Rev. Mod. Phys.* **1945**, *17*, 323−342.
(70) Goychuk, I. In *Advances in Chemical Physics*; Rice, S. A., Dinner, A. R., Eds.; Wiley: 2012; Vol. *150*, pp 187−253.
(71) Min, W.; Luo, G.; Cherayil, B. J.; Kou, S. C.; Xie, X. S. Observation of a power-law memory kernel for fluctuations within a single protein molecule. *Phys. Rev. Lett.* **2005**, *94*, 198302.
(72) Tang, J.; Lin, S.-H. Distance versus energy fluctuations and electron transfer in single protein molecules. *Phys. Rev. E* **2006**, *73*, 3597−10.
(73) Satija, R.; Das, A.; Makarov, D. E. Transition path times reveal memory effects and anomalous diffusion in the dynamics of protein folding. *J. Chem. Phys.* **2017**, *147*, 152707−9.
(74) Pressé, S. A data-driven alternative to the fractional Fokker−Planck equation. *J. Stat. Mech.: Theory Exp.* **2015**, *2015*, P07009.
(75) Waskasi, M. M.; Gerdenis; Moore, A. L.; Moore, T. A.; Gust, D.; Matyushov, D. V. Marcus bell-shaped electron transfer kinetics observed in an Arrhenius plot. *J. Am. Chem. Soc.* **2016**, *138*, 9251−9257.
(76) Yang, H.; Luo, G.; Karnchanaphanurach, P.; Louie, T.-M.; Rech, I.; Cova, S.; Xun, L.; Xie, X. S. Protein conformational dynamics probed by single-molecule electron transfer. *Science* **2003**, *302*, 262−266.
(77) Kou, S. C.; Xie, X. S. Generalized Langevin equation with fractional Gaussian noise: Subdiffusion within a single protein molecule. *Phys. Rev. Lett.* **2004**, *93*, 180603.
(78) Min, W.; English, B. P.; Luo, G.; Cherayil, B. J.; Kou, S. C.; Xie, X. S. Fluctuating enzymes: Lessons from single-molecule studies. *Acc. Chem. Res.* **2005**, *38*, 923−931.
(79) Wang, Y.; Zocchi, G. The folded protein as a viscoelastic solid. *EPL (Europhysics Letters)* **2011**, *96*, 18003.
(80) Xie, X. S. Enzyme kinetics, past and present. *Science* **2013**, *342*, 1457−1459.
(81) Engelkamp, H.; Hatzakis, N. S.; Hofkens, J.; De Schryver, F. C.; Nolte, R. J. M.; Rowan, A. E. Do enzymes sleep and work? *Chem. Commun.* **2006**, *327*, 935−6.
(82) Lin, C.; Sepunaru, L.; Kätelhön, E.; Compton, R. G. Electrochemistry of single enzymes: Fluctuations of catalase activities. *J. Phys. Chem. Lett.* **2018**, *9*, 2814−2817.
(83) Grossman-Haham, I.; Rosenblum, G.; Namani, T.; Hofmann, H. Slow domain reconfiguration causes power-law kinetics in a two-state enzyme. *Proc. Natl. Acad. Sci. U. S. A.* **2018**, *115*, 513−518.
(84) Davia, F. G.; Herrera, S. E.; Calvo, E. J. Gaussian distribution of electron transfer distance in redox terminated self-assembled thiol monolayers. *J. Phys. Chem. C* **2019**, *123*, 13939−13943.
(85) Zusman, L. D. Outer-sphere electron transfer reactions at an electrode. *Chem. Phys.* **1987**, *112*, 53−59.
(86) Zhang, B.; Song, W.; Pang, P.; Lai, H.; Chen, Q.; Zhang, P.; Lindsay, S. Role of contacts in long-range protein conductance. *Proc. Natl. Acad. Sci. U. S. A.* **2019**, *116*, 5886−5891.

DOI: 10.1021/acs.jpcb.9b04516
J. Phys. Chem. B XXXX, XXX, XXX−XXX